

Micro Thermocouple and Voltage Sensor for Fuel Cell Real Time Interior Monitoring

Chi-Yuan Lee*, Shuo-Jen Lee, Yi-Man Lo, Yun-Min Liu

Department of Mechanical Engineering, Yuan Ze Fuel Cell Center, Yuan Ze University, Taoyuan, Taiwan

*E-mail: cylee@saturn.yzu.edu.tw

Received: 13 September 2013 / *Accepted:* 23 October 2013 / *Published:* 15 November 2013

The temperature and voltage distribution in membrane electrode assembly (MEA) importantly affect the performance of fuel cell. Conventional methods can only get the interior information of fuel cell by modeling or invasive measurement. By using micro-electro-mechanical systems (MEMS) for fabricating micro flexible thermocouple, resistance temperature detector (RTD) and voltage sensor, this work uses polyimide (PI) film (50 μ m) as a flexible substrate, it is small enough to place anywhere between MEA and flow channel, and no support frame is required. Therefore, the micro sensors that integrated into the fuel cell have the advantage of multi-function, high accuracy, high linearity, high sensitivity, extreme flexibility, mass production and short response time. Integrated micro sensors are embedded in a fuel cell to determine the temperature and voltage parameters in the inner flow channel of a fuel cell. Users can monitor the interior temperature and voltage distribution in the flow channel of a fuel cell.

Keywords: MEMS, micro RTD sensor, micro thermocouple and voltage sensors

1. INTRODUCTION

With the extensive use of fuel cell, some key issues need to be addressed. Water thermal management is key to the fuel cell performance [1-3], the temperature status and voltage distribution of membrane electrode assembly (MEA) and internal fuel conditions play a very significant role [4, 5]. However, the impact level of the products from the reaction on fuel cell performance and life service is unknown. Therefore, the real time monitoring of the internal temperature and voltage parameters of the fuel cell is an important issue. Cho [6] used the software package ESI-Computational fluid dynamics (ESI-CFD) in simulation to explore the relationship between flow channel internal heat distribution and fuel cell performance. David [7] placed optical fiber on the bipolar plate of the fuel cell to measure the temperature in real time. Ali [8] made T-shape thin film thermocouple on the polyimide (PI)

substrate to measure the high temperature proton exchange membrane fuel cell (PEMFC). Gagliardo [9] developed an array sensor on the Teflon substrate and the placed the circuit board between the flow field plate and pressing plate of the fuel cell to measure the temperature distribution of various points of the fuel cell by using the signal acquisition system. The comparative analysis of the internal voltage of the fuel cell was conducted by using the neutron radiation images. As for the design and manufacturing of thermocouple, resistive temperature sensors by previous studies are as described as below: Chu [10] designed a micro thermocouple on the silicon chip. Wrbanek [11] used ceramics as the substrate and four materials to combine with the platinum pad to develop four types of high temperature thermocouples for comparison. Mohammadi [12] developed a resistance temperature detector (RTD) on the silicon chip. Chung [13] used SiO₂ as the substrate to develop the resistive micro sensor.

In order to avoid micro sensors embedded within the fuel cell to take up too much reaction area, this study used the micro-electro-mechanical systems (MEMS) technology to integrate the flexible micro thermocouple and RTD and voltage sensors, and PI as a flexible substrate. It is small volume and can thus be embedded in any place inside the fuel cell. Moreover, it does not require designing any support framework, and the integrated micro sensor has advantages such as small size, multi-function, high accuracy, high linearity, high sensitivity, flexibility, batch manufacturing, and short response time. By using the integrated micro sensor in the fuel cell to measure internal temperature and voltage parameters, the users can monitor and adjust the temperature and voltage of the fuel cell in real time to improve performance and service life.

2. METHODOLOGY AND DESIGN OF MICRO SENSOR

2.1. Theory and Design of Thermocouple and Voltage Sensor

In 1821, Thomas Seebeck found that when two wires of different metals are connected to form the circuit, a circuit is formed at the sensing end by connecting the two metallic wires. As shown in figure 1, when the two connection points of the thermocouple are in contact with different temperatures, different diffusion currents will be generated inside the metal due to different diffusion rates of the electrons, resulting in a current inside the metallic connection circuit. The multiplication of the net current value with the contact resistance of the metallic point can result in a tiny open circuit voltage in the circuit known as Seebeck electromotive force as defined in Eq. (1). The voltage of the thermocouple is the function of the temperature difference of the two points. Seebeck coefficient (α_s) is defined as:

$$\alpha_s = \frac{(V_1 - V_2)}{(T - T_0)} \quad (1)$$

where, the open-circuit voltage is:

$$V_T = V_1 - V_2 \quad (2)$$

Therefore, we can infer:

$$V_T = V_1 - V_2 = \alpha_{s1}(T - T_0) - \alpha_{s2}(T - T_0) = (\alpha_{s1} - \alpha_{s2})(T - T_0) \quad (3)$$

By measuring the voltage difference and referring to temperature difference, we can obtain the actual temperature.

The sensing materials of the micro thermocouple are gold and nickel, as the Seebeck coefficients of gold (6.5) and nickel (-15) are great and the sensing area is not affected by output voltage. The size design is relatively more flexible and the linewidth of the sensor tip is designed as $60\mu\text{m}$. The late stage conductor linewidth is $210\mu\text{m}$ to enhance the strength.

The micro voltage sensor in this study is resistive type. Its electrode type is of a thin conductor electrode structure, and the sensing area is $250\mu\text{m}\times 250\mu\text{m}$. The principle is to use the two thin conductive wires to contact both ends of the object to be measured before applying a stable power on the object to measure the difference between the voltages of the two thin conductive wires [14].

The integrated design diagram of the micro thermocouple and voltage sensor is as shown in figure 2.

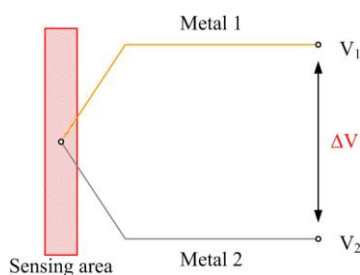


Figure 1. Schematic diagram of thermocouple.

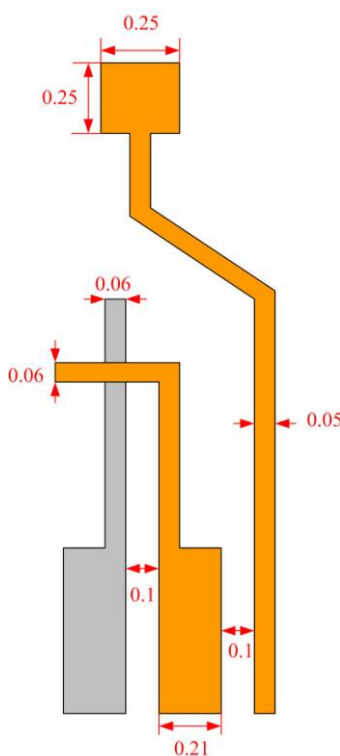


Figure 2. Integrated design diagram of micro thermocouple and voltage sensor (unit: mm).

2.2. Theory and Design of RTD Sensor

The resistance of a general metal wire is represented by Eq. (4).

$$R = \rho \frac{L}{A} \tag{4}$$

where ρ denotes resistivity (Ωm); L is length of the metal wire (m); and A is the cross-sectional area of the wire (m^2).

The resistivity of most metallic conductors can rise over the rising environment temperature, this is caused by the conductor’s “resistance-temperature coefficient” as defined in Eq. (5).

$$\alpha = \frac{1}{\rho_0} \frac{d\rho}{dT} \tag{5}$$

where α is the resistance-temperature coefficient; ρ_0 is the resistivity at 0°C .

If the RTD sensor is used in the linear range of the resistance, it can be expressed by Eq. (6).

$$R_t = R_0 (1 + \alpha_1 \Delta T) \tag{6}$$

As for the micro RTD sensor, the sensing area is $390\mu\text{m} \times 400\mu\text{m}$, the minimum linewidth is $10\mu\text{m}$ as shown in figure 3.

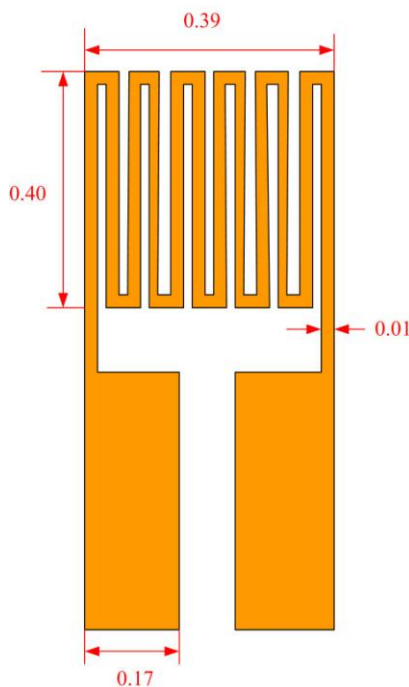


Figure 3. Design diagram for micro RTD sensors (unit: mm).

3. FABRICATION OF MICRO SENSORS

In this study, the micro sensors were made by using the surface micromachining technology. The procedures included deposition, lithography, lift-off and wet etching. The process details are as shown below.

3.1. Fabrication of Micro Thermocouples and Voltage Sensors

The fabrication processes of the micro thermocouples, and voltage sensors are as shown in Fig. 4. The detailed steps are as described as follows: (a) Particles on the PI film surface are removed by acetone and methanol; (b) after the coating of photoresist (PR), the patterns are exposed; (c) use the e-beam evaporator to evaporate nickel; (d) use the lift-off to place the specimen in the acetone for about one hour before using methanol and DI water for cleaning; (e) repeat Step (b), define the patterns of the metal and micro voltage sensors of the second layer of the micro thermocouple; (f) use the e-beam evaporator to evaporate the gold as the material of the second layer micro thermocouple and micro voltage sensors; (g) after taking out the specimen, use the lift-off method to place the specimen in the acetone for about one hour before using the using methanol and DI water for cleaning; (h) micro sensors are coated with photoresist as the protection layer.

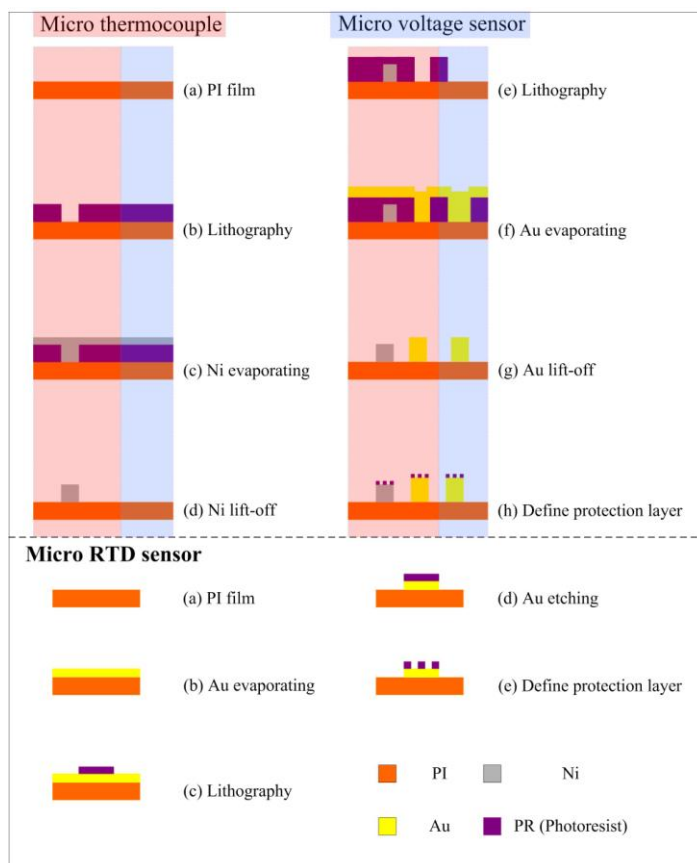


Figure 4. Manufacturing process of the micro sensors.

3.2. Manufacturing Process of Micro RTD Sensors

The manufacturing processes of the micro RTD sensors are as shown in figure 4. The detailed steps are described as follows: (a) Particles on the PI film surface are removed by acetone and methanol; (b) use the e-beam evaporator to evaporate chromium and gold as the adhesion layer and the electrode

layer; (c-d) micro sensors are patterned by lithographic and wet etching process; (e) photoresist (PR) is spin coated as the protection layer, and the pad is exposed by lithography process to complete the micro RTD sensor.

4. FUEL CELL INTERNAL LOCALIZED DIAGNOSIS

We also know that people always choose TGA to analyze the temperature in fuel cell [15]. This study embedded the integrated micro sensors inside the fuel cell and measured the localized reactions of the fuel cell. The embedded place was the upstream of the flow channel of the cathode (air inlet), midstream and downstream (air outlet) as shown in figure 5. There were a group of micro thermocouples and a group of micro RTD sensors in the upstream, midstream and downstream. A micro voltage sensor was placed at the downstream.

After installing the membrane electrode assembly with the micro sensors inside the fuel cell, a performance test was measured by using a 100W/A fuel cell and an integrated fuel cell test station (850C). Before the test, the flexible micro sensors were calibration before connecting with NI to capture the resistance of the micro RTD sensor, the voltage of the micro thermocouple and the voltage of the micro voltage sensor to monitor and analyze the changes.

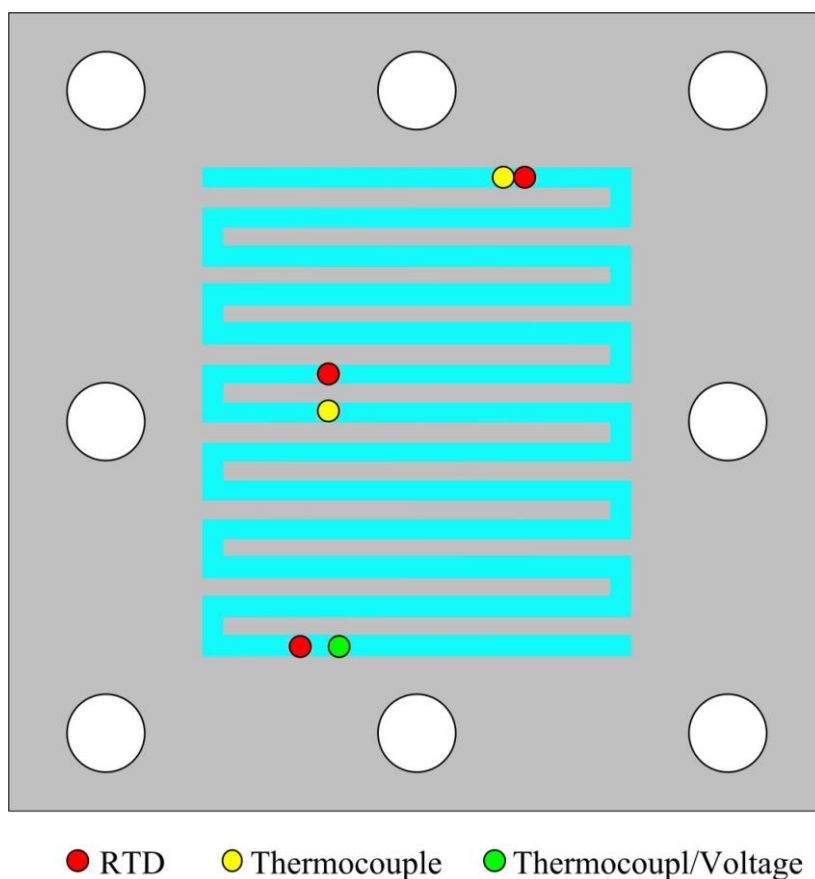


Figure 5. Schematic diagram of the actual measurement data points.

4.1. Measurement Results of the Output of the Constant Current at 12A

Under the condition of cell temperature at 65°C, the cathode and anode were humidified at 100% RH for 30 min when the constant current was at 12A. The flow volume of hydrogen and air was 1.2 times of that of the anode and 3 times of that of cathode respectively.

4.2. Temperature Real Time Monitoring

Under the condition of constant current at 12A and output for 30 min, real-time monitoring was conducted on the temperature. The temperature curves of the fuel cell test station (850C) and the micro temperature sensor measurement are as shown in figures 6 to 8. For the three temperatures, the internal temperatures of the upstream, and midstream and downstream of the flow channel have no difference from the cell temperature as recorded in the fuel cell test station (850C). The possible causes are:

1) As the current is not great, the reactions at the upstream, midstream and downstream are not significant; therefore, the internal temperature and external thermocouple measurement of temperature have not great difference.

2) The downstream internal temperature is slightly higher than the internal temperature of the upstream and downstream of the flow channel possibly because the downstream reaction is more significant than that of the midstream or the upstream. The significant reaction can result in the increase in temperature. Hence, the downstream temperature is more significant than that of the upstream or the midstream of the flow channel [16]. This is consistent with the inference of general fuel cell theory that the downstream reaction is relatively more significant. The comprehensive comparison diagram is as shown in figure 9.

3) After the operation of the fuel cell for about 20~25 min, the internal and external temperatures reached the stable state.

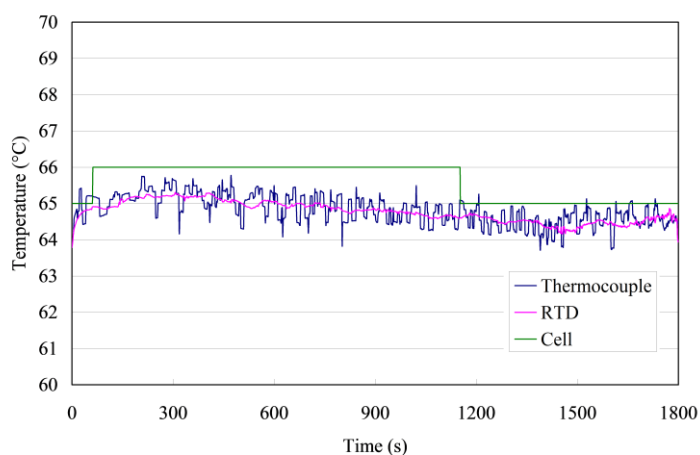


Figure 6. Trends of the upstream temperature for cell temperature at 65°C and constant current at 12A.

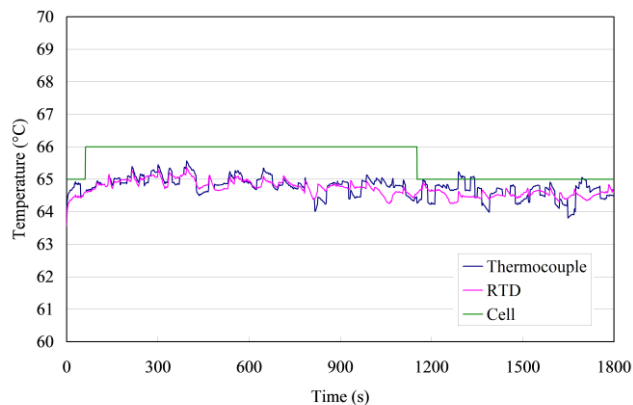


Figure 7. Trends of the midstream temperature for cell temperature at 65°C and constant current at 12A.

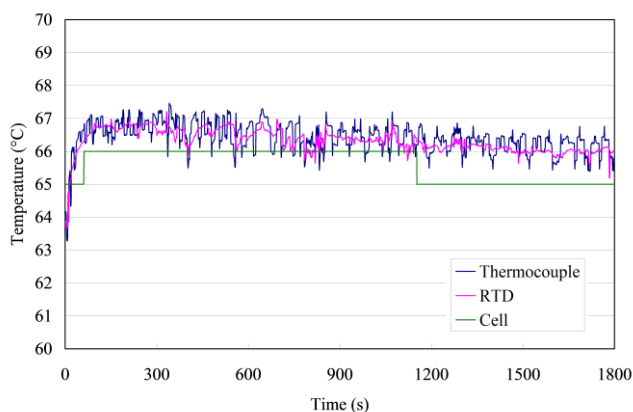


Figure 8. Trends of the downstream temperature for cell temperature at 65°C and constant current at 12A.

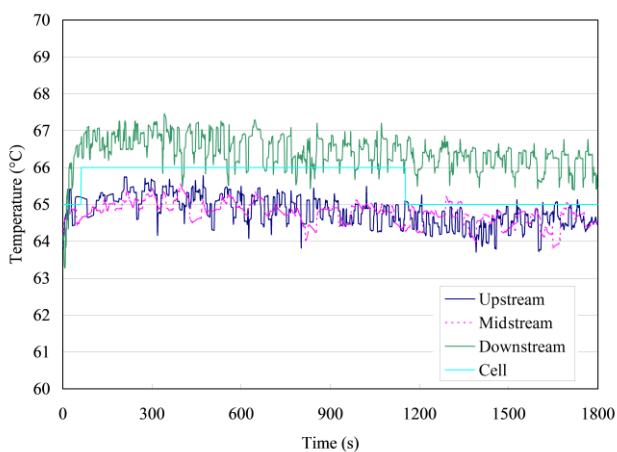


Figure 9. Comparison of upstream, midstream and downstream temperatures in case of the constant current at 12A.

4.3. Real Time Monitoring of Voltage

As shown in figure 10, for the constant current at 12A and output time at 30 min, by comparing the internal and external voltage of the fuel cell, the internal voltage value of the membrane electrode assembly is slightly higher than the external measurement of the voltage. As the electric power is mainly generated by the membrane electrode assembly, parts of the voltage have been lost when the voltage is transferred from the membrane electrode assembly to the bipolar plate. As the small current reaction is not significant, the voltage gap is less than 1mV.

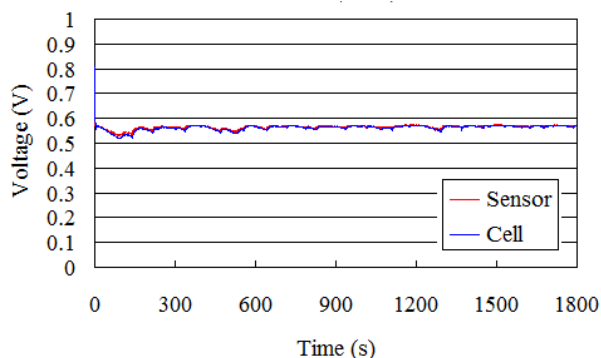


Figure 10. Trends of the voltage in case of the cell temperature at 65°C and constant current at 12A.

5. CONCLUSION

This study successfully used the micro-electro-mechanical systems technology to develop the integrated micro sensor for the internal real time monitoring of fuel cell. The micro sensor has advantages of multiple function, high accuracy, high linearity, high sensitivity, tough flexibility, batch manufacturing and rapid response time.

ACKNOWLEDGEMENTS

This work was accomplished with much needed support and the authors would like to thank for the financial support by National Science Council of R. O. C. through the grant NSC 102-2221-E-155-033-MY3, NSC 100-2628-E-155-002-MY2, NSC 102-2622-E-155-003 and NSC 102-2622-E-155-006. The authors also like to thank Professors Shih-Hung Chan, Ay Su, Fangbor Weng and Guo-Bin Jung for their valuable advice and assistance in experiment. In addition, we would like to thank the YZU Fuel Cell Center and NEMS Common Lab for providing access to their research facilities.

References

1. C. Bao, M. Ouyang and B. Yi; *Int J Hydrogen Energ.* 31 (2006) 1040-1057.
2. Y. Zong, B. Zhou and A. Sobiesiak; *J Power Sources* 161 (2006) 143-159.
3. L. Matamoros and D. Bruggemann; *J Power Sources* 161 (2006) 203-213.
4. W. Vielstich, H. A. Gasteiger and A. Lamm, *Handbook of fuel cells: Fundamentals technology and applications*, John Wiley & Sons Inc, 2003.

5. H. Nishikawa, R. Kurihara, S. Sukemori, T. Sugawara, H. Kobayasi, S. Abe, T. Aoki, Y. Ogami and A. Matsunaga; *J Power Sources* 155 (2006) 213-218.
6. S. A. Cho, P. H. Lee, S. S. Han and S. S. Hwang; *J Power Sources* 178 (2008) 692-698.
7. N. A. David, P. M. Wild, J. Hu and N. Djilali; *J Power Sources* 192 (2009) 376-380
8. S. T. Ali, J. Lebakb, L. P. Nielsen, C. Mathiasen, P. Møller and S. K. Kær; *J Power Sources* 195 (2010) 4835-4841.
9. J. J. Gagliardo, J. P. Owejan, T. A. Trabold and T. W. Tighe; *J Power Sources* 605 (2009) 115-118.
10. D. Chu, W. K. Wong, K. E. Goodeson and R. F. W. Pease; *J Vac Sci Technol. B* 30 (2003) 2985-2989.
11. J. D. Wrbanek, G. C. Fralick and D. Zhu; *Thin Solid Film* 520 (2012) 5801-5806.
12. A. R. Mohammadi, T. C. M. Graham, C. P. J. Bennington and M. Chiao; *Sensor Actuat A-Phys.* 163 (2010) 471-480.
13. G. S. Chung and C. H. Kim; *Microelectr J* 39 (2008) 1560-1563.
14. C. Y. Lee, W. Y. Fan and W. J Hsieh; *Sensors* 10 (2010) 6395-6405.
15. M. Lee, S. B. Khan, K. Akhtar, H. Han and J. Seo; *Int. J. Electrochem. Sci.* 8 (2013) 4225- 4233.
16. M. Wang, H, Guo and C, Ma; *J Power Sources* 157 (2006) 1181-187.